atmosphere

Article

Tree-Ring-Based Drought Reconstruction in Northern North China over the Past Century

Yanchao Wang [1,2,3,*], Huifang Zhang [4,*], Hui Wang [5], Jingli Guo [5], Erliang Zhang [5], Jun Wang [5], Xiao Li [5], Haoliang Wei [5] and Changliang Zhou [5]

1 College of Bioscience and Engineering, Xingtai University, Xingtai 054001, China
2 State Key Laboratory of Loess and Quaternary Geology, Institute of Earth Environment, Chinese Academy of Sciences, Xi'an 710075, China
3 Hebei Key Laboratory of Digital Freshwater Aquaculture Technology, Xingtai University, Xingtai 054001, China
4 College of Mathematics and Information Technology, Xingtai University, Xingtai 054001, China
5 Mulan-Weichang Forestry Administration of Hebei Province, Weichang 068450, China; wanghui1272@163.com (H.W.); zrzykfyly@126.com (J.G.); yljgywh@126.com (E.Z.); wangjun999521@163.com (J.W.); lixiao713@163.com (X.L.); weihaoliang2022@163.com (H.W.); zhouchagliang@163.com (C.Z.)
* Correspondence: wang.yan.chao@stu.xjtu.edu.cn (Y.W.); 201420440@xttc.edu.cn (H.Z.)

Abstract: A tree-ring width chronology was developed from the Chinese pine (*Pinus tabuliformis*) in northern North China. To acquire a long-term perspective on the history of droughts in this region, the Standardized Precipitation Evapotranspiration Index (SPEI) from August of the previous year to February of the current year was reconstructed for the period of 1903–2012 AD. The reconstruction explained 46.6% of the instrumental records over the calibration period of 1952–2012. Five dry periods (1916–1927, 1962–1973, 1978–1991, 1994–1999 and 2002–2005) and three wet periods (1908–1915, 1928–1961 and 1974–1977) were found in the reconstructed period, and most of the dry years (periods) in the reconstruction were supported by historical records. Comparisons between the reconstruction and other nearby dryness/wetness indices and precipitation reconstructions demonstrated a good repeatability and high reliability in our reconstruction. Spatial correlation implied that the reconstruction could represent regional hydroclimatic characteristics on a larger regional scale. Significant periodicities and correlations were observed between the reconstructed data and the quasi-biennial oscillation (QBO), El Niño–Southern Oscillation (ENSO) and Pacific Decadal Oscillation (PDO), which suggested that the hydroclimatic variation in northern North China may be closely connected to remote oceans. The significant and high correlation between the reconstructed series and sea surface temperatures (SSTs) in the eastern equatorial and Southeast Pacific Ocean indicated that ENSO may be the main factor influencing the regional climate.

Keywords: North China; Chinese pine; tree ring; SPEI; drought reconstruction

check for updates

Citation: Wang, Y.; Zhang, H.; Wang, H.; Guo, J.; Zhang, E.; Wang, J.; Li, X.; Wei, H.; Zhou, C. Tree-Ring-Based Drought Reconstruction in Northern North China over the Past Century. *Atmosphere* **2022**, *13*, 482. https://doi.org/10.3390/atmos13030482

Academic Editor: Bryan C. Weare

Received: 22 January 2022
Accepted: 11 March 2022
Published: 15 March 2022

1. Introduction

During recent decades, global warming has been expected to intensify atmospheric circulation and hydrological circles [1], which would cause the redistribution of precipitation and evapotranspiration [2]. Furthermore, changes in precipitation and evapotranspiration affect the balance of the surface water budget and result in more frequent hydroclimatic extremes [3], such as droughts and floods in many regions of the world [4–6].

The hydroclimatic extremes may cause changes in growth or death of trees [7], and climate change information can be recorded in tree rings. In response to the global warming crisis, it is very important to understand the response of tree rings from specific species to meteorological factors and drought events.

Chinese pine is an endemic species and is widely distributed in China. It plays an important role in ecological conservation and regional socioeconomic development. Chinese pine forests are the main landscape and have been greatly affected by climate change in northern North China. Therefore, it is considered suitable for studying the effect of climate on its growth and reconstructing paleoclimate. However, due to the different habitat conditions, the response of Chinese pine to meteorological factors may vary. For example, in China, the main factor affecting Chinese pine growth is precipitation in Kalaqin [8], temperature in Weichang [9] and Standardized Precipitation Evapotranspiration Index (SPEI) in the Taihe Mountains [10]. The precipitation and SPEI are directly related to droughts, while a temperature rise markedly affects the severity of droughts through evapotranspiration [11]. In general, the low annual tree growth is caused by drought.

Drought is one of the most significant and challenging climatic disasters as a response to global climate change in arid and semiarid regions [12,13] and exerts a severe impact on water-dependent economic activities, populations and livelihoods, natural ecosystems and especially agricultural production [14,15]. Therefore, it is very important to further investigate the long-term characteristics of drought variations for efficient water management and adaptation to climate change.

To understand drought changes, many studies based on tree-ring data have addressed long-term precipitation variations in North China [8,16–20]. However, one of the main disadvantages of previous studies was that the effect of evapotranspiration was neglected. In fact, the variations in evapotranspiration caused by temperature or other meteorological factors have had a remarkable effect on dry and wet conditions over the past decades [21].

The SPEI is a multiscalar drought index based on the monthly (or weekly) difference between precipitation and potential evapotranspiration (PET), which is used for determining the onset, duration and magnitude of drought conditions in a variety of natural and managed systems [11]. PET can cause large water losses from water bodies and soil. Soil water losses will also affect runoff, river discharge and groundwater storage, which can lead to drought. Due to considering the effect of PET on drought severity, the multiscalar SPEI will be able to identify the different drought types and effect in the context of global warming [11]. A number of studies have analyzed and evaluated drought events by the SPEI in different regions of the world [22–24]. Several drought reconstructions based on the SPEI from tree rings have been published in China [10,25,26] and other countries [27–29]. However, no reconstructed studies have investigated drought changes using the SPEI in the Weichang Manchu and Mongolian Autonomous County (Weichang) in northern North China, which is environmentally sensitive and ecologically fragile [30].

The objectives of this study were (1) to develop a new tree-ring chronology in northern North China, (2) to investigate the tree growth–climate relationship and reconstruct a seasonal drought history over the past 110 years using tree-ring width in Weichang in North China and (3) to explore the potential triggers of drought variation in the study area.

2. Materials and Methods

2.1. Study Area

The study area is located in northern North China on the upper reaches of the Luanhe River, with a semimoist, semiarid monsoon climate typical of temperate continents. Based on the meteorological records from the Weichang station, the annual mean temperature generally ranges from 3.1 to 6.5 °C. The annual mean precipitation is from 237 to 684 mm, with most of precipitation falling from June to September. The annual mean relative humidity is approximately 56%. The area is an important green ecological barrier preventing sandstorms in Beijing and Tianjin and is also a vital water catchment for the Luanhe River.

2.2. Tree-Ring Data

The sampling site (41°42′ N, 117°04′ E, 966 m a.s.l.) is in the Mengluan Forest Farm (ML) (Figure 1) in Weichang in northern North China. It is covered with thick soil and has high canopy density. The dominant tree species are *Pinus tabuliformis* and *Larix gmelinii.* The woodland's owners gave us permission to collect the samples and took part in the study as the paper's coauthors, and field work permits were not required. According to the International Tree-Ring Data Bank (ITRDB) standard, two or three cores were collected from each tree. A total of 48 cores from 23 living Chinese pines were taken by increment borers. The sampled trees were generally growing on a northeast-facing topographic aspect, with slopes ranging from 10° to 40°.

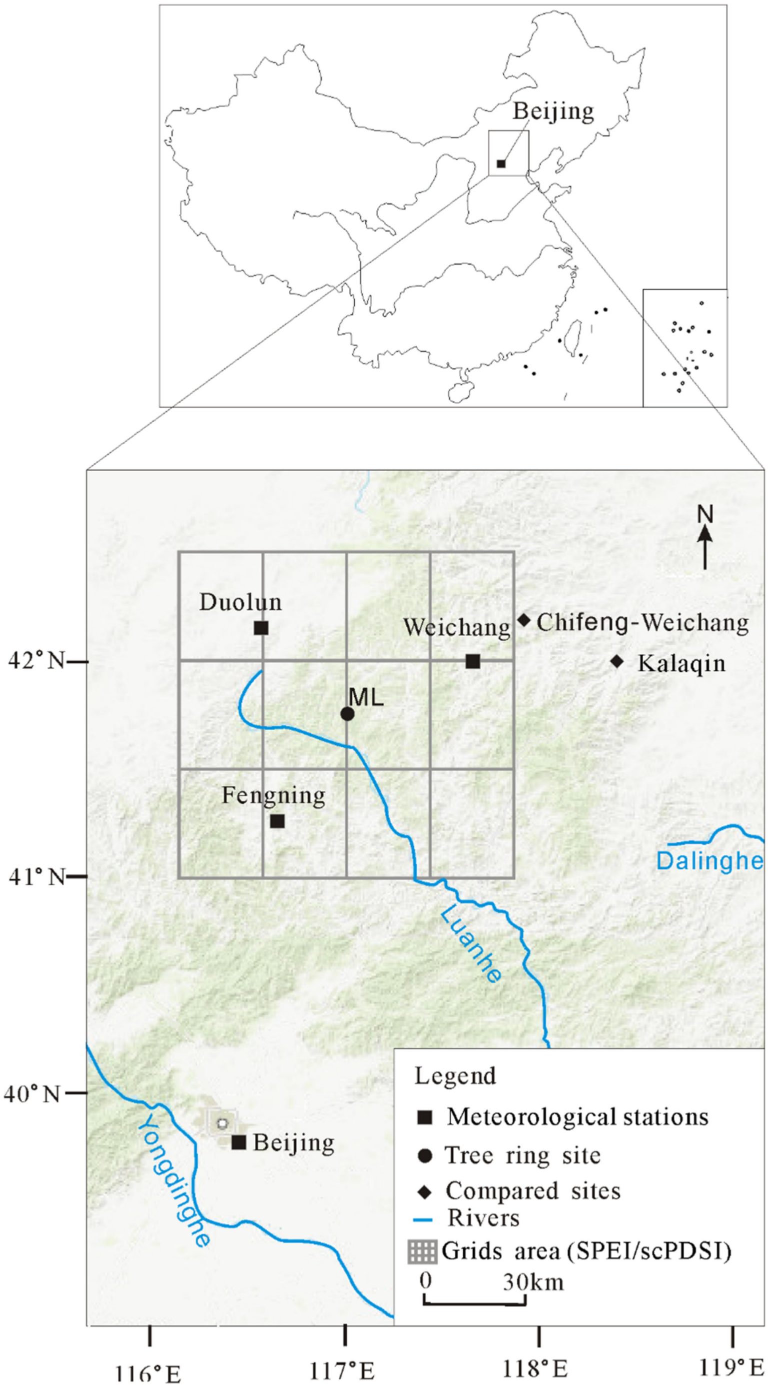

Figure 1. Map of the sampling site. The final figure was modified from a base map created using the USGS National Map Viewer (public domain): http://viewer.nationalmap.gov/viewer/, accessed on 15 November 2021.

The original samples were pretreated according to the standard dendrochronological techniques [31,32] and measured to the nearest 0.001 mm using the LINTAB (Frank Rinntech, Heidelberg, Germany) measuring system. The COFECHA program (https://www.ltrr.arizona.edu/pub/dpl/, accessed on 21 April 2021) [33] was utilized to evaluate the quality of the cross-dating of the tree-ring series. The results showed that the series intercorrelation of all raw series was 0.736, with a mean sensitivity of 0.328 and an absent ring rate of zero. The ARSTAN program (https://www.ltrr.arizona.edu/pub/dpl/, accessed on 21 April 2021) [34] was employed to develop the final tree-ring chronology. To remove biological growth trends and conserve the common low-frequency climatic signal, negative exponential or linear regression curves were employed to fit each ring width measurement series. Finally, we obtained three types of chronologies: standard (STD) chronology, residual (RES) chronology and ARSTAN (ARS) chronology. In further analysis, the RES chronology was used in the study because it preserved high-quality high-frequency signals and could display high-frequency oscillation characteristics [35]. A subsample signal strength (SSS) [36] higher than 0.85 was used to determine the most reliable period, which corresponded to a minimum sample depth of five cores from 1903 AD (Figure 2).

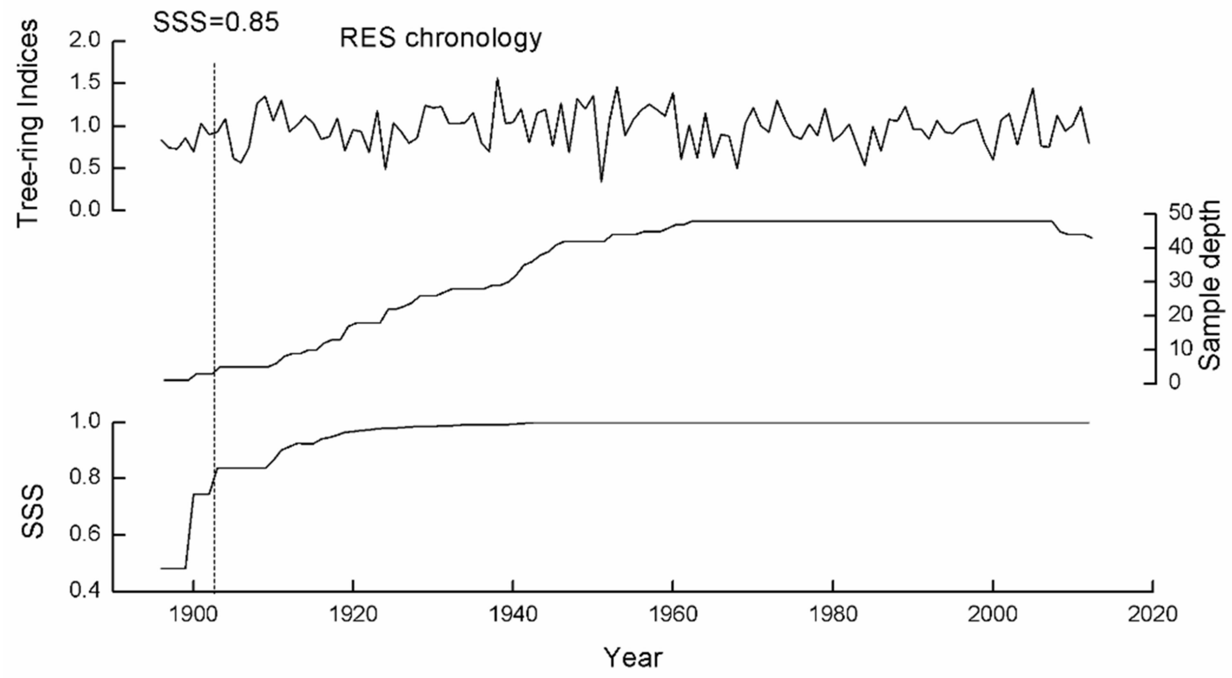

Figure 2. Tree-ring RES chronology, SSS and sample depth.

2.3. Climatic Data

Local monthly precipitation and temperature data were collected from the Weichang (41°56′ N, 117°45′ E; 842.8 m a.s.l., 1951–2012), Fengning (41°13′ N, 116°38′ E; 661.2 m a.s.l., 1956–2012) and Duolun (42°11′ N, 116°28′ E; 1245.4 m a.s.l., 1952–2012) meteorological stations (Figure 1), which were located near the sampling site. The relative altitudes between the three meteorological stations and the sampling site were −123.2 m, −304.8 m and 279.4 m, respectively. Weichang and Fengning meteorological stations were located in the north of Yanshan, while Duolun meteorological station was located on the southern edge of Inner Mongolia plateau. The mean monthly precipitation and temperature patterns of these three stations have synchronous variations (Figure 3a). The changes in the meteorological data of the three stations were similar (Figure 3b,c). Preliminary analyses showed that random errors and obvious uneven distributions for either temperature or precipitation were not present in the meteorological records from the three stations. Meanwhile, the annual climatic factors of these three stations were highly correlated (Table 1). Therefore, the arithmetic averages of the data records from these meteorological stations were chosen to represent the regional climate information during the instrumental period.

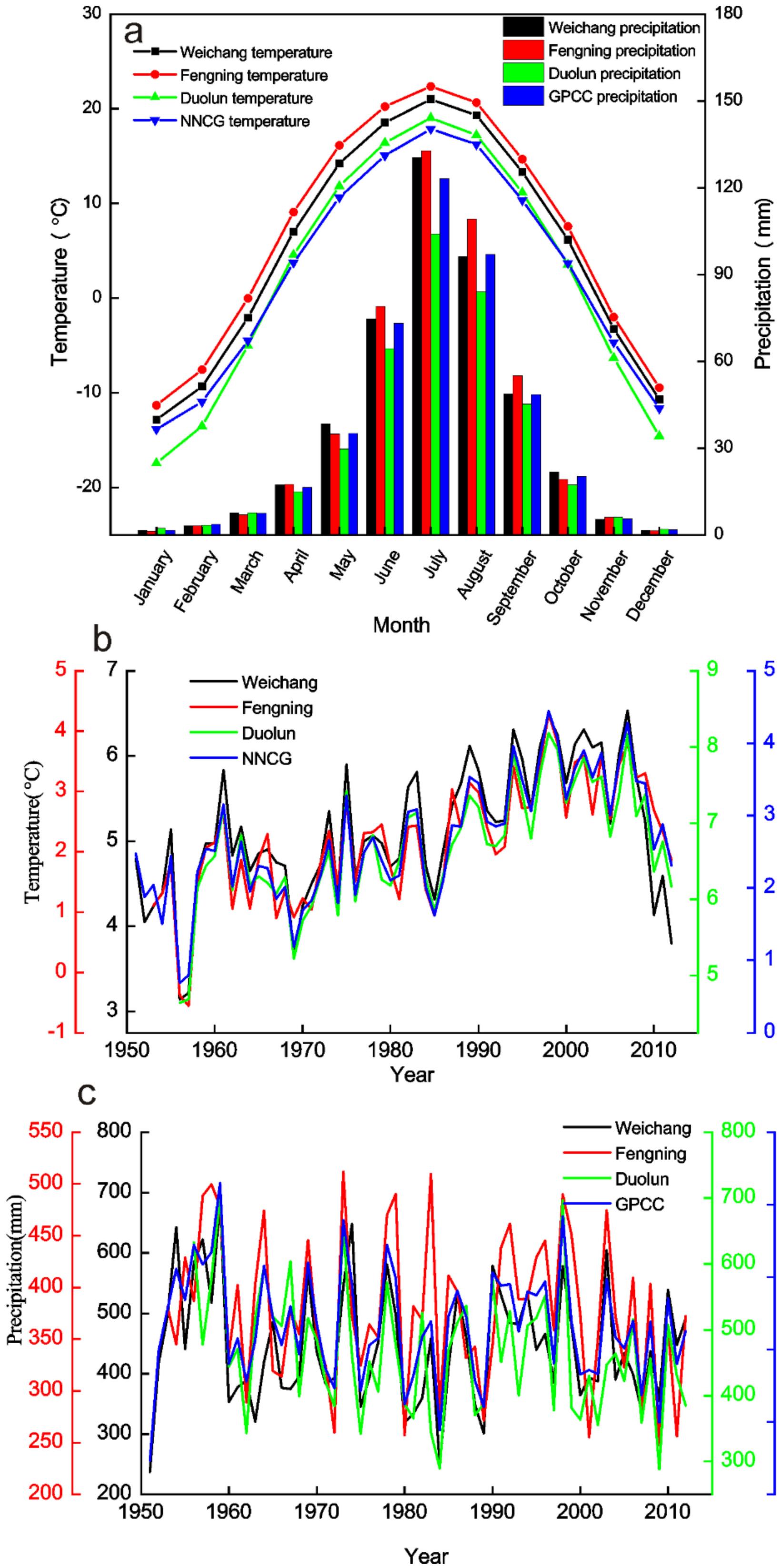

Figure 3. (**a**) The monthly mean temperature and precipitation, (**b**) The mean temperature records (**c**) The annual precipitation records at from the Duolun, Weichang and Fengning stations, and the Climate Research Unit temperature (NOAA NCEP CPC GHCN_CAMS gridded dataset (NNCG)) and precipitation (Global Precipitation Climatology Centre (GPCC)).

Table 1. Correlation matrix of the annual climatic factors of three stations.

Item		Weichang	Fengning	Duolun
Temperature correlation	Weichang	1	0.885 **	0.957 **
	Fengning		1	0.930 **
	Duolun			1
Precipitation correlation	Weichang	1	0.562 **	0.600 **
	Fengning		1	0.564 **
	Duolun			1

** Significant at the 0.01 level (2-tailed).

Long-term instrumental precipitation records from the Beijing (39°48′ N, 116°28′ E; 31.3 m a.s.l., 1905–2012) meteorological station, approximately 220 km south of the sampling site, were available to verify our reconstruction. However, some records during certain times were absent due to wars or other reasons. The missing values were estimated by the linear interpolation method.

To determine the combined effects of temperature and precipitation, we also estimated the relationship between the ring widths and the self-calibrating Palmer Drought Severity Index (scPDSI) data. Using the global 0.5° gridded scPDSI database, the monthly scPDSI values of 12 grid points (https://www.uea.ac.uk/web/groups-and-centres/climatic-research-unit/data, accessed on 18 December 2021) [37] covering the three stations' areas were obtained from the near sampling site. The center coordinates of 12 grid points were composed of the latitude (41°15′ N, 41°75′ N and 42°15′ N,) and longitude (116°15′ E, 116°45′ E, 117°15′ E and 117°45′ E), forming a cross matrix. The final monthly scPDSI values were the arithmetic average of the data from 12 grid points. In addition, the global scPDSI database was driven by a preliminary version of the CRU TS monthly climate dataset. In CRU TS, due to few or no meteorological station observations, some grid cell climate values were relaxed towards the 1961–1990 period, which means that the scPDSI values of grid cells may be closer to zero and anomalously dry or wet conditions may be underestimated in regions and times with poor data coverage. Most meteorological records started from the 1950s in China, so the scPDSI values before the 1950s may cause uncertainty. For the reliability and stability, the monthly scPDSI data from 1951–2012 were utilized because the meteorological data from Weichang stations were available from 1951.

The SPEI drought monitor data were calculated based on the mean temperature data from the NOAA NCEP CPC GHCN_CAMS gridded dataset (NNCG) (https://ftp.cpc.ncep.noaa.gov/wd51yf/GHCN_CAMS/, accessed on 16 January 2022) and the monthly precipitation data from the Global Precipitation Climatology Centre (GPCC) (http://climexp.knmi.nl, accessed on 16 January 2022). And the PET was estimated by the Thortnthwaite equation. The climate data from NNCG and GPCC were represented in the area between 41°N to 42°30′ N and 116°E to 118°E, which cover three stations area. The climate data changes were similar with the meteorological data of the three stations (Figure 3). Regional SPEI were directly extracted from the SPEI global drought monitor da-taset (http://sac.csic.es/spei/index.html, accessed on 20 December 2021) [11]. The period for the SPEI is 1951 to 2012, with timescales between 1 and 48 months. The multiscalar SPEI could represent the different effects of water availability on tree growth in particular periods/seasons in tree-ring analyses and might cause different responses during drought reconstructions. It is important to choose the appropriate SPEI timescales [38,39]. To identify the major environmental signals that influence tree growth, the SPEI at the 1-month scale was used to estimate additional variations in drought. Considering that the climate in year t-1 affects ring width in the following year t [32], the SPEI data records from July of the previous year through October of the current year were selected to identify the climatic effects on the radial growth of Chinese pine in the study region.

2.4. Statistical Methods

Correlation analyses were utilized to evaluate the climate–growth relationship between the RES chronology and climate variables during the observation period. Considering the lag effect due to tree growth [32], climate variables within the time window from July of the previous year to the October of the current year and seasonal combinations were included in the analyses. Based on the results of the tree growth–climate relationship, a simple linear regression model was designed to reconstruct the limiting climatic factors. The stability and reliability of the model were assessed via the split-sample method [40,41]. The statistical parameters included the Pearson's correlation coefficient (r), coefficient of determination (r^2), product means (t), sign test (ST), reduction of error (RE) and coefficient of efficiency (CE).

To reveal the temporal and spatial representativeness of the SPEI reconstruction, spatial correlations between both the reconstructed and observed SPEI with the global gridded SPEI dataset were conducted according to the KNMI Climate Explorer (http://climexp.knmi.nl, accessed on 16 January 2022) over the period of 1951–2012. Spatial correlations were also calculated between the reconstructed SPEI data and the gridded Hadley Centre Sea-ice and Sea-surface Temperature Data Set Version 1 (HadISST1) temperature using the same method during the period of 1903–2012. Comparisons of the reconstructed SPEI with other hydroclimatic records were further processed to verify the temporal and spatial representativeness of the reconstruction. The multitaper method (MTM) was employed to detect the natural cycles in the reconstruction.

Additionally, to investigate the historical characteristics of dry and wet climatic changes, extremely dry/wet years were defined as those years that were greater/less than the mean $\pm$ 2δ of the SPEI reconstruction, and the severely dry/wet years were determined by using the same methods with the threshold mean $\pm$ δ [10,25,42]. The natural variability of Earth's climate could be explained over interannual, decadal, centennial, millennial and other timescales. The decadal scale has been the primary interest in paleoclimate studies. Previous studies have revealed that the low-frequency variation in the reconstruction is more reliable than the high-frequency variation [43]. To highlight decadal scale variation, an 11-year moving average was applied in data analysis [44]. The study area is a transitional zone from semimoist to semiarid monsoon climate with a varied climate. Due to the East Asian monsoon, extreme flood and drought events frequently occurred and had a strong influence on agricultural production and human lives, as well as on the ecosystems [13]. Based on the vagaries of climate and the relevant references [9,10,42], on a decadal scale, the time interval in which the SPEI value was lower/higher than the mean of the reconstructed values and lasted for more than 3 years was defined as the dry/wet period.

3. Results

3.1. Climate–Growth Response

The correlations between the RES chronology and monthly precipitation and average temperature (1956–2012 AD) at the three meteorological stations are shown in Figure 4. The RES chronology showed positive correlations with precipitation in almost all the months, and is particularly significant in August ($p < 0.05$) and September ($p < 0.01$) and November ($p < 0.01$) of the previous year, and February of the current year ($p < 0.05$) (Figure 4). Significant negative correlations were observed for the RES chronology and temperature in August ($p < 0.01$) of the previous year, and May ($p < 0.01$) and June ($p < 0.01$) of the current year (Figure 4). On a seasonal scale, after combining several monthly variables, the RES chronology was most strongly positively correlated with the monthly average precipitation from August of the previous year to June of the current year ($r = 0.567$, $p < 0.01$) and negatively correlated with the average temperature from May–June of the current year ($r = -0.486$, $p < 0.01$) (Figure 4).

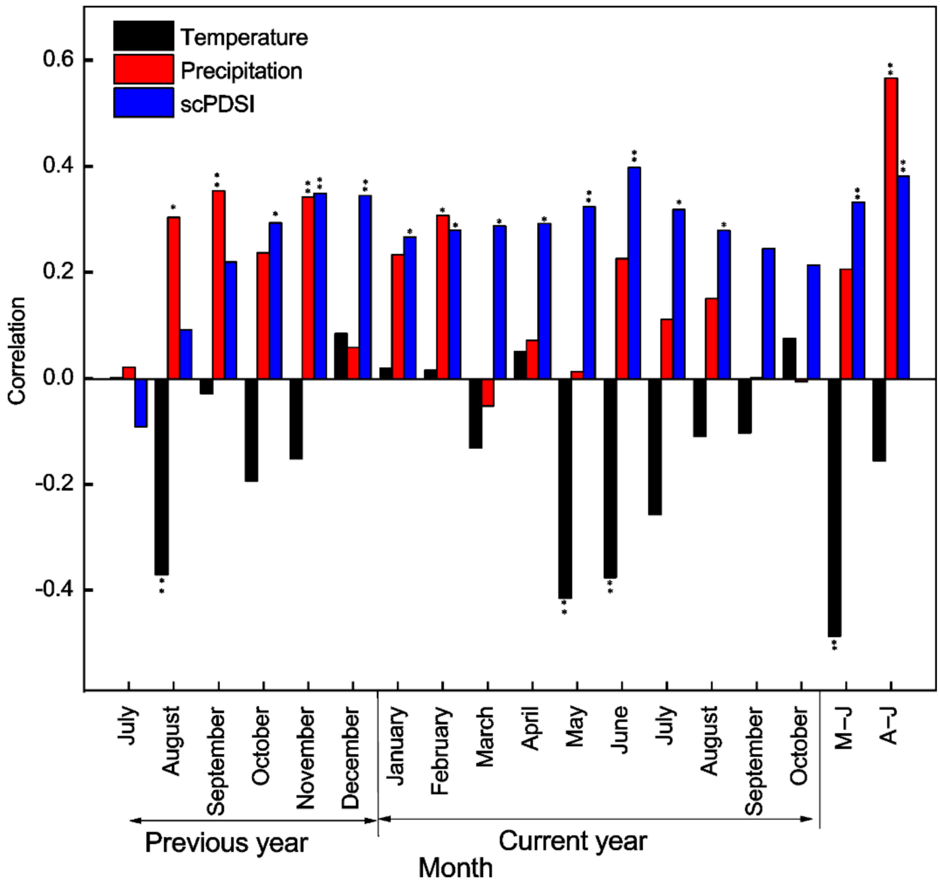

Figure 4. Correlations between tree-ring RES chronology and monthly mean temperature and scPDSI, monthly total precipitation.* and ** represent significance at the 95 and 99% confidence limits; M–J: May to June; A–J: August of the previous year to June of the current year.

For scPDSI, the calculations showed that the RES chronology was positively correlated with scPDSI in almost all the months except July of the previous year and the highest correlation was observed in June ($r = 0.399$, $p < 0.001$) of the current year. After months of combination, all correlation coefficients data were lower than that in June of the current year (Figure 4). These results mean that the RES chronology is not suitable for scPDSI reconstruction in our research region.

In addition, the RES chronology showed positive correlations with the SPEI data in some months, except in July of the previous year, and March, April and October of the current year (Figure 5), indicating that tree growth was severely limited by sustained water deficits [45]. For the single-month SPEI, the highest correlation was found with the SPEI in September of the previous year ($r = 0.376$, $N = 61$, $p < 0.001$) (Figure 5), which was too low for accurate reconstruction. Using the seasonally averaged SPEI variables, the SPEI at the 1-month scale from August of the previous year to the February of the current year ($SPEI_{82}$) had the highest significant correlation with the RES chronology ($r = 0.683$, $N = 61$, $p < 0.001$) (Figure 5). Therefore, in the following analysis, we concentrated on the $SPEI_{82}$.

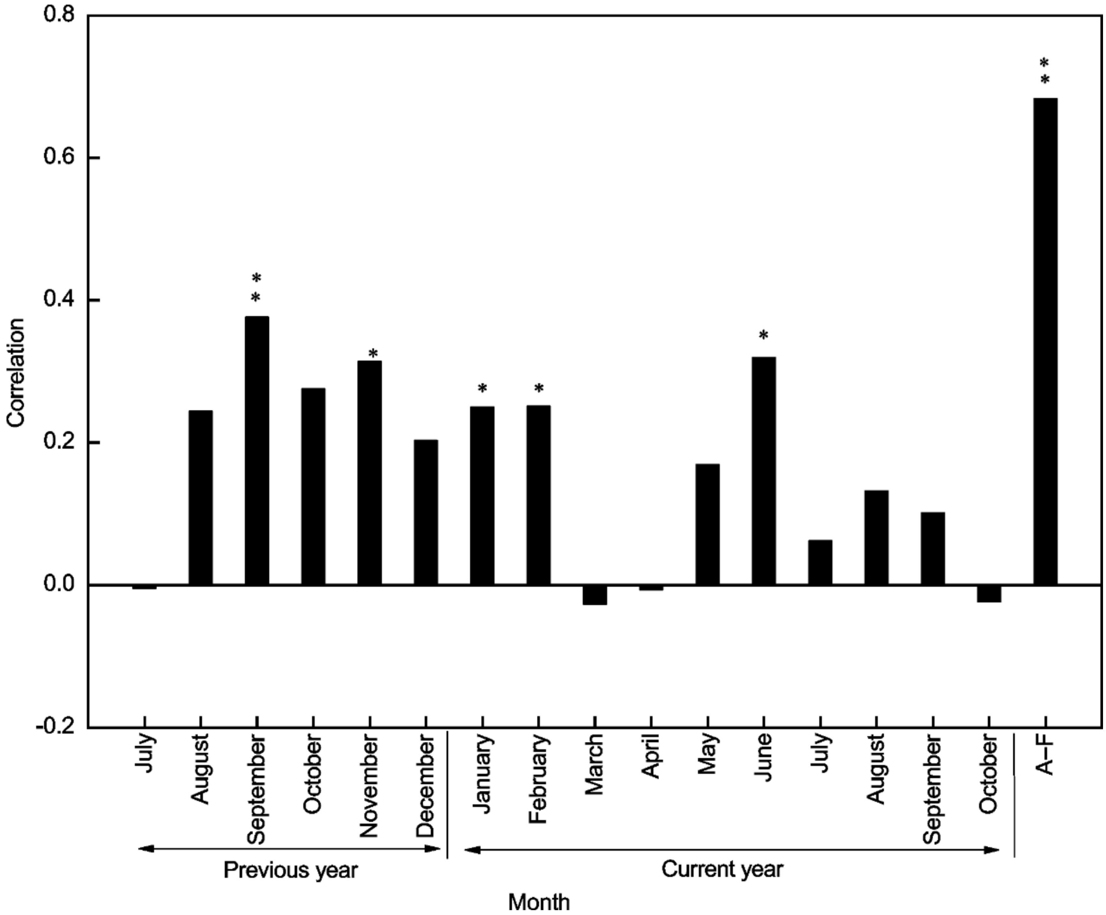

Figure 5. Correlations between the RES chronology and monthly SPEI data (1951–2012 AD). * and ** represent significance at the 95 and 99% confidence limits; A–F: August of the previous year to February of the current year.

3.2. Transfer Function and Verification

Based on the distinct response relationships between the RES chronology and climate variables, the mean $SPEI_{82}$ could be calculated using the following function: $SPEI_{82} = 1.287 \times W_i - 1.259$ where $SPEI_{82}$ represents the average SPEI from August of the previous year to February of the current year at the 1-month scale; W_i represents the tree-ring index at year *i*. The reconstructed $SPEI_{82}$ was very close to the observed data (Figure 6a), and the model could explain 46.6% (45.7% after factoring out degrees of freedom) of the actual $SPEI_{82}$ variance during the calibration period of 1952–2012.

The results of the split-sample test showed that the ST from the calibration and verification period from the calibration were statistically significant ($p < 0.05$), and all other parameters were extremely statistically significant ($p < 0.01$) (Table 2). Furthermore, positive RE and CE values confirmed the validity and reliability of the transfer function [40].

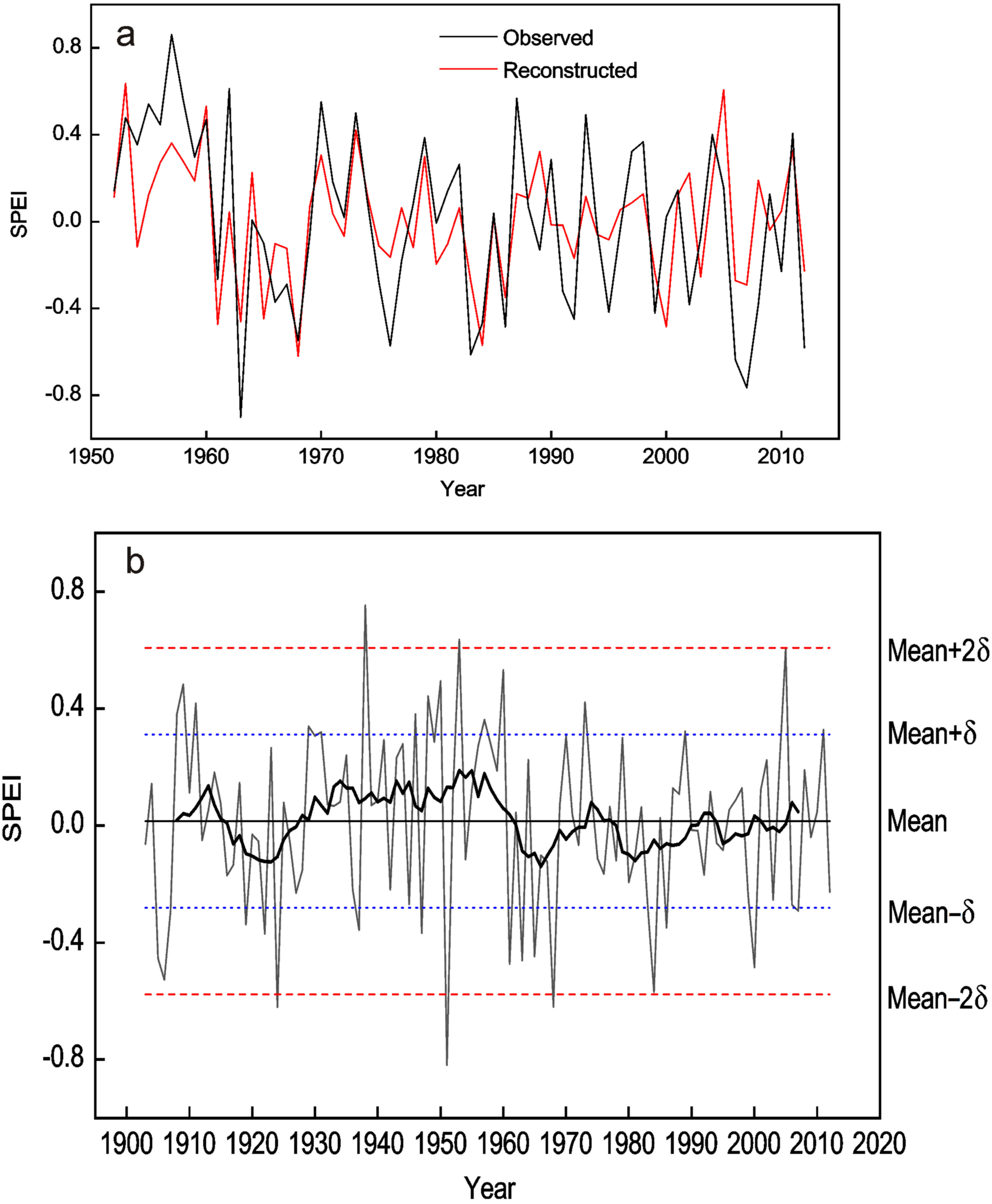

Figure 6. The observed and reconstructed $SPEI_{82}$. (**a**) Comparison between the reconstructed (red line) and observed (black line) $SPEI_{82}$ from 1952–2012. (**b**) The reconstructed $SPEI_{82}$ (the bold line represents an 11-year moving average).

Table 2. The results of split calibration–verification procedure.

Calibration				Verification						
Period	r	r^2	t	**Period**	r	r^2	*RE*	*CE*	*ST*	t
1952–1981	0.773 **	0.598	3.944 **	1982–2012	0.572 **	0.327	0.348	0.169	23+/8− *	3.661 **
1983–2012	0.571 **	0.327	3.791 **	1951–1982	0.772 **	0.597	0.533	0.402	23+/8− *	3.852 **
1951–2012	0.683 **	0.466	5.070 **	–	–	–	–	–	–	–

r: Pearson's correlation coefficient; r^2: coefficient of determination; t: product means; *ST*: sign test; *RE*: reduction of error; *CE*: coefficient of efficiency. ** Significant at the 0.01 level (2-tailed). * Significant at the 0.05 level (2-tailed). –: No data.

3.3. SPEI Reconstruction

Based on the above function, the monthly mean $SPEI_{82}$ variations in the Weichang region for the period of 1903 to 2012 were reconstructed (Figure 6b). In Figure 6b, the mean value and standard deviation (σ) of the $SPEI_{82}$ reconstruction for the past 110 years are 0.015 and 0.296, respectively. According to the dry and wet standards described in the Section 2 above, the reconstruction series consisted of 77 normal years, 14 severely dry years, 14 severely wet years, 3 extremely dry years and 2 extremely wet years, which currently represent approximately 70.00%, 12.73%, 12.73%, 2.73% and 1.82% of the entire reconstruction series, respectively. The three extremely dry years were 1924, 1951 and 1968, and the two extremely wet years were 1938 and 1953 (Figure 6b).

Normally, the long-term sustainability of dry or wet conditions has a strong effect on every aspect of social economics. Thus, the multiyear continuous dry or wet periods were analyzed for the last century based on the $SPEI_{82}$ reconstruction. Five dry periods lasting over three years were found from 1916–1927, 1962–1973, 1978–1991, 1994–1999 and 2002–2005, and three long-lasting wet periods were found from 1908–1915, 1928–1961 and 1974–1977 (Figure 6b). For all periods, the interval from 1978–1991 was the longest existing dry period (14 years, 12.73% of the total reconstruction period), whereas the period from 1928 to 1961 was the longest wet period (34 years, 30.91% of the total reconstruction period), with the most elevated mean $SPEI_{82}$.

3.4. Spatial Representativeness and Periodicities

Further spatial correlation fields showed that the reconstructed and observed $SPEI_{82}$ had a significant and positive correlation with the current SPEI pattern in northern North China (Figure 7a,b), and the fields of greatest correlation covered a vast geographical area in the transitional belt of Northeast and North China.

The MTM analysis showed that the reconstructed $SPEI_{82}$ contained 2.01-year, 2.37-year, 2.94-year, 3.36-year and 3.59-year interannual cycles, and 18.62-year multidecadal cycles at a 90% significance level (Figure 8).

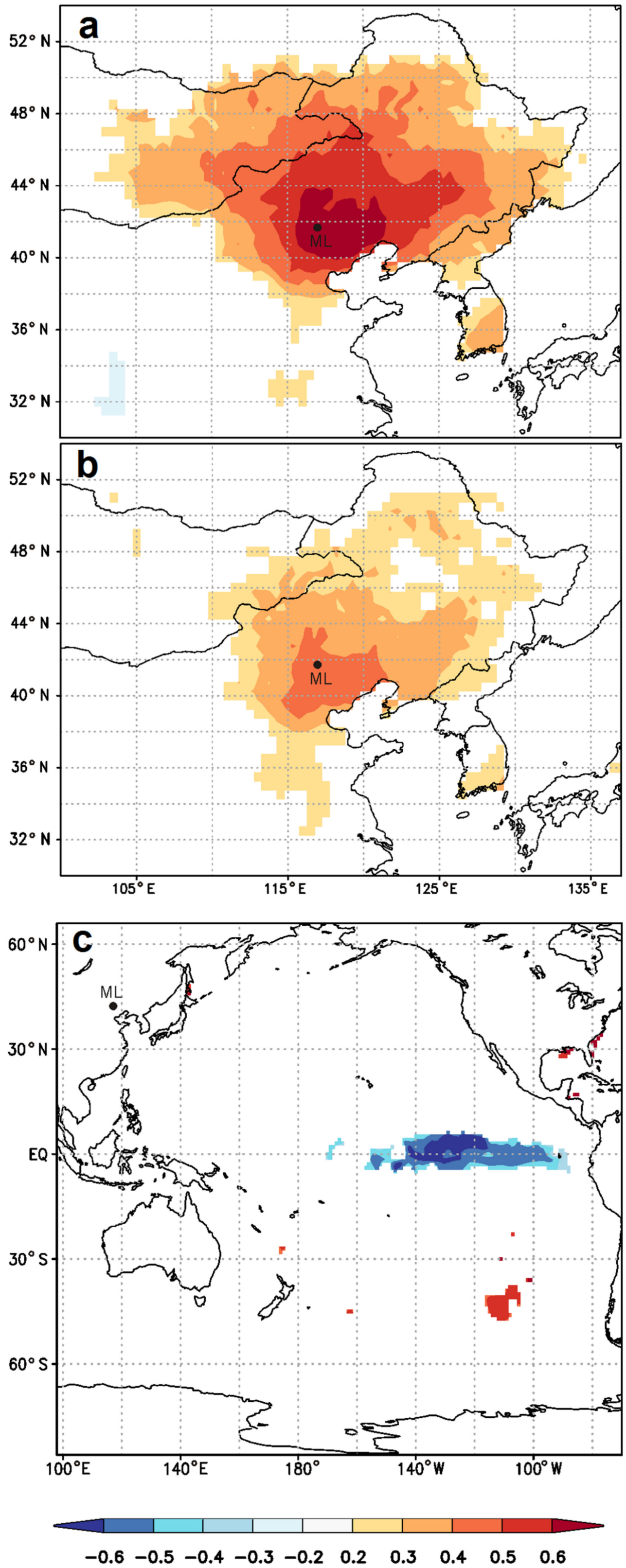

Figure 7. Patterns of field correlation ($p < 0.1$). (**a**) Observed gridded mean $SPEI_{82}$ series with the gridded mean August–February SPEI (the grid system is 0.5° × 0.5°) at the 1-month scale. (**b**) Reconstructed $SPEI_{82}$ in our study with the gridded mean August–February SPEI of the previous year. (**c**) Reconstructed $SPEI_{82}$ with the gridded the May–November HadISST1 1° reconstruction of the previous year (11-year running mean) from 1903 to 2012. The sampling site is marked by a black dot.

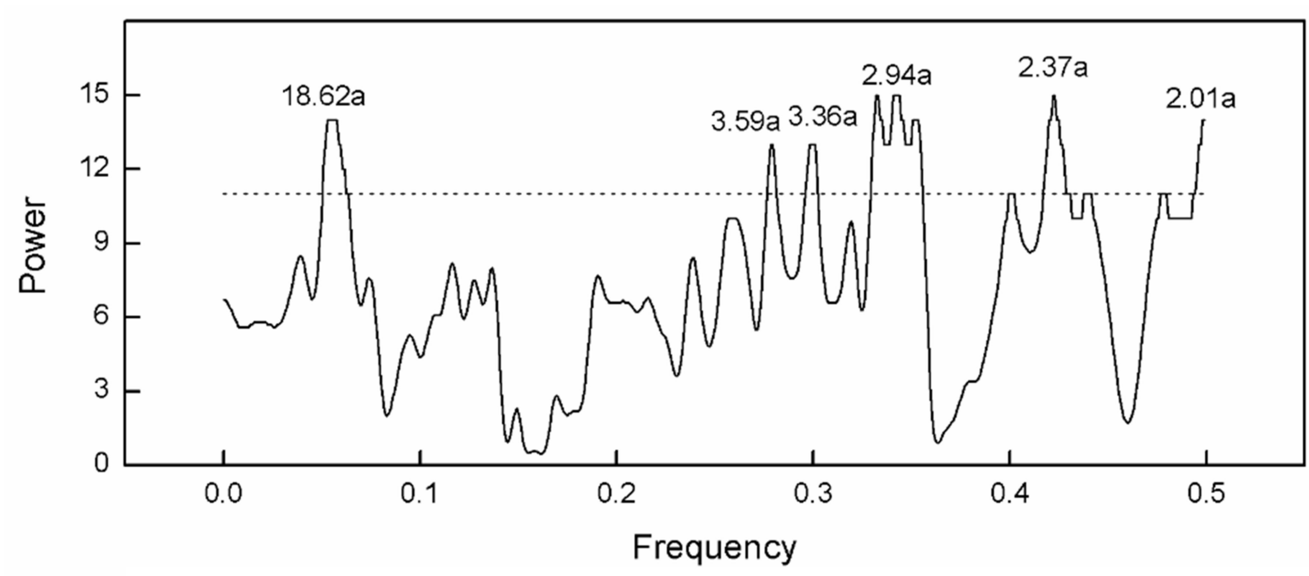

Figure 8. MTM spectral density of the reconstruction. The dashed line represents the 90% confidence level. a: year.

4. Discussion

4.1. Climate–Growth Relationship

The RES chronology was significantly correlated with precipitation and temperature in most months. This result might be explained by the fact that rainfall (in August and September of the previous year) and the snowfall (in November of the previous year and February of the current year) could improve the soil water condition of the root environments for tree growth in the current year [46], whereas high temperature (in August of the previous year and May and June of the current year) might increase the intensity of soil evaporation and tree transpiration, and cause water deficits for trees, forming a narrow ring in the current year [47]. Overall, the climate–growth response was positively correlated with precipitation and negatively correlated with temperature, demonstrating that moisture stress was the main factor influencing the growth pattern of Chinese pine in the study region [18]. This pattern was also found in other dendroclimatic studies in semiarid and arid zones [9,17,18]. The significant positive correlation between the RES chronology and the scPDSI and SPEI further confirmed our conclusion. After seasonal combinations, the most highly significant positive correlations ($p < 0.001$) were found between the RES chronology and the precipitation from August of the previous year to June of the current year (Figure 4), which suggested that the radial growth of Chinese pines in northern North China was primarily affected by precipitation. However, these correlations were too low for accurate reconstruction. In addition, after combining the monthly SPEI variables, the highest correlation occurred at a 1-month scale during the period from August of the previous year to the February of the current year ($r = 0.683$, $N = 62$, $p < 0.001$), indicating that the precipitation and PET in the summer and fall of the previous year and in the winter of the current year were the most important factors that influenced the radial growth of trees in the region.

4.2. Comparison with Other Proxy Records

The characteristics of the $SPEI_{82}$ reconstruction at various spatial and temporal scales were obtained by comparisons with other hydroclimatic data. According to the results of the spatial correlations (Figure 7a,b), the dryness/wetness indices at Doulun (which is near the study area) and the drought events from historical records and the average SPEI (which is from the Global SPEI database and date back to 1901) from August of the previous year to February of the current year from the 12 grid points (SPEIm) (http://climexp.knmi.nl, accessed on 16 January 2022) covering the three stations and the long-term instrumental precipitation records from the Beijing meteorological station and two available precipitation reconstructions based on tree-ring width from Chifeng-Weichang [18] and Kalaqin [8] were considered to explore dryness/wetness fluctuations.

The dryness/wetness indices derived from historical documents [48–50] provided a tool to validate the reliability of tree-ring-based climate reconstructions, and the indices were further divided into five grades: very wet, wet, normal, dry and very dry, which corresponded to values ranging from 1 to 5, respectively [48]. The dryness/wetness indices of Doulun were employed for further analysis. Comparisons showed that the reconstructed $SPEI_{82}$ series displayed some similar trends to the dryness/wetness indices at the decadal scale ($r = -0.608$, $N = 81$, 1915–1995, $p < 0.001$) (Figure 9a). However, it was noteworthy that some remarkable differences in the periods of 1923–1927, 1957–1966 and 1993–1995 were discovered between the two series. The discrepancies might have resulted from microclimate changes in our study region or omissions and inconsistencies in the historical records. A similar phenomenon also occurred in other dendrochronological studies [18,29].

According to the definition of the SPEI, higher/lower SPEI values mean stronger degrees of moisture/drought. Therefore, drought years (or periods) often had lower SPEI values. Based on the observed average climate data of the three meteorological stations, the reconstructed $SPEI_{82}$ was significantly negatively correlated with the precipitation from August of the previous year to February of the current year ($r = -0.535$, $N = 57$, $p < 0.001$). Meanwhile, a historical document [51] and meteorological data in Hebei Province showed that there were 22 severe drought years after 1920, and 16 of them (accounting for 66.67% of the total) corresponded with $SPEI_{82}$ values that were lower than the average values of the whole reconstructed $SPEI_{82}$ series (Figure 9b). Moreover, the extremely dry years in 1951 and 1968 were consistent with the drought events from historical records (Figure 9b).

The reconstructed $SPEI_{82}$ series was significantly positively correlated with the $SPEI_m$ and the precipitation from August of the previous year to February of the current year from the Beijing meteorological station and the reconstructed precipitation from August of the previous year to July of the current year from Chifeng-Weichang [18] and Kalaqin [8] on an annual scale, with $r = 0.316$ ($p < 0.001$, $N = 110$, 1903–2012), $r = 0.343$ ($p < 0.001$, $N = 107$, 1905–2012), $r = 0.549$ ($p < 0.001$, $N = 101$, 1903–2003) and $r = 0.471$ ($p < 0.019$, $N = 106$, 1903–2008), respectively. On a decadal scale, the dry and wet intervals of the five curves showed some similar trends with different magnitudes (Figure 9c). Common dry intervals occurred in the late 1910s–1920s, early 1960s–early 1970s, late 1970s–early 1990s, late 1990s and early 2000s; wet intervals occurred in the early 1910s, late 1920s–early 1960s and mid-1970s. Notably, the dry interval in the early 1960s–early 1970s was observed in all three series, and was the driest interval in our study area in the last century. Furthermore, the dry intervals of the early 1960s–early 1970s and the late 1970s–early 1990s from the reconstructed $SPEI_{82}$ series were also found to be shorter rainfall periods in the observed annual precipitation data from the 17 meteorological stations in North China [52]. Severe drought in the 1920s was also revealed in northern China [16,17,53].

The results above indicated that the dryness/wetness variations were at a regional scale and that the reconstructed $SPEI_{82}$ could reflect a large-scale hydroclimatic signal in the northern part of China. This feature was also confirmed by spatial correlation (Figure 7a,b). In general, the reconstructed $SPEI_{82}$ captured these drought events or periods well in northern China.

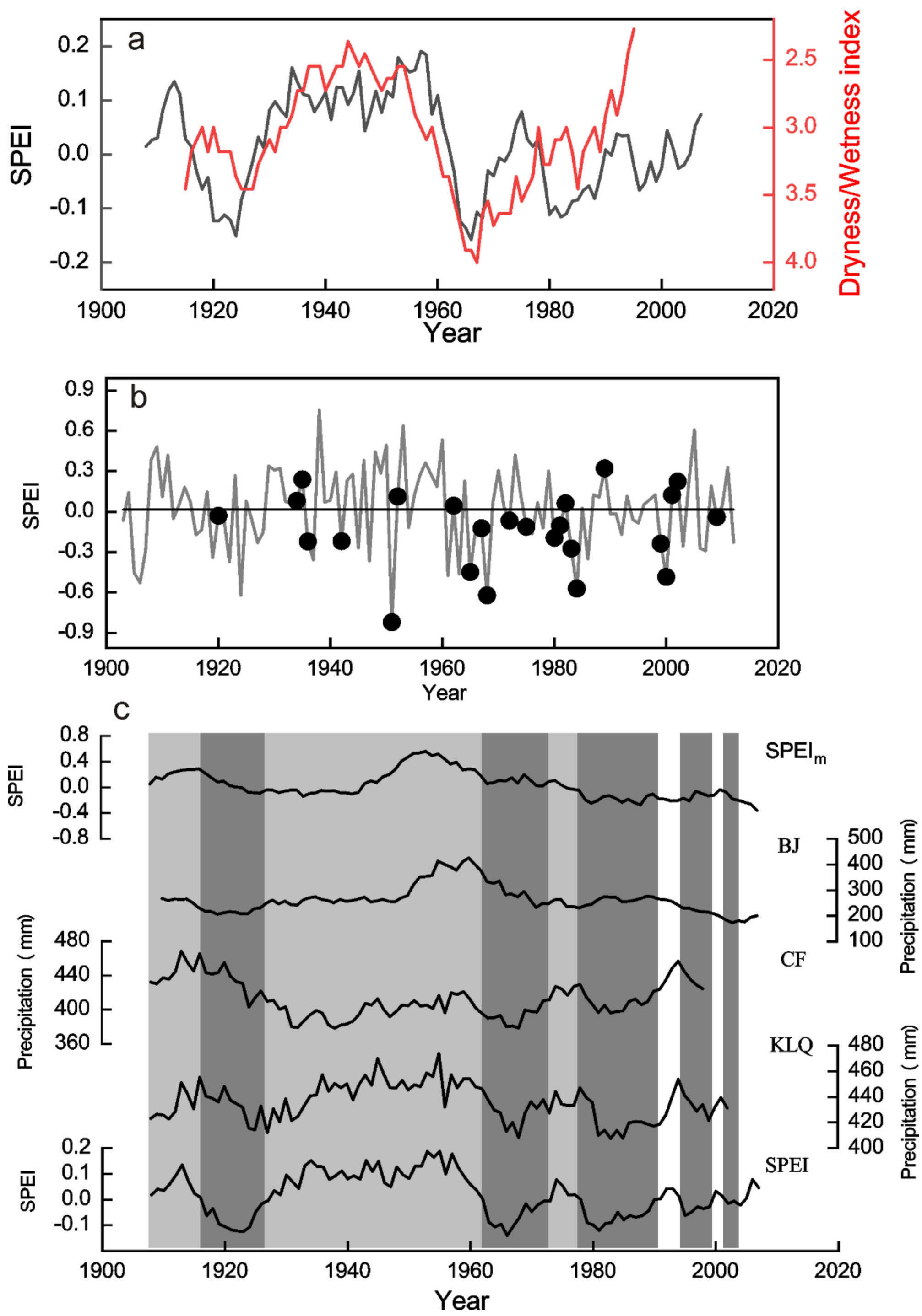

Figure 9. Comparisons with other proxy records. (**a**) Comparison between the $SPEI_{82}$ reconstruction (black line) and dryness/wetness indices at Duolun (red line). (**b**) Comparison between the $SPEI_{82}$ reconstruction and drought events (dots) (horizontal line is the averaged $SPEI_{82}$ from 1903 to 2012). (**c**) Comparison of the average SPEI from August of the previous year to February of the current year from the 12 grid points (SPEIm) (http://climexp.knmi.nl, accessed on 16 January 2022) covering the three stations, the precipitation observations from August of the previous year to February of the current year from the Beijing meteorological station (BJ), the precipitation from August of the previous year to July of the current year at Chifeng-Weichang (CW) and Kalaqin (KLQ) and the $SPEI_{82}$ reconstruction (SPEI). (The smoothed line is an 11-year moving average, and the dark/light gray shadow areas represent the same dry/wet periods in different series).

4.3. Periodicities and Teleconnection

The MTM analysis showed some significant cycles in the reconstructed $SPEI_{82}$ series, which demonstrated that the dryness/wetness conditions may be influenced by other factors in addition to those discussed above. The significant high-frequency peaks of 2.01 years, 2.37 years and 2.94 years were close to the quasi-biennial oscillation (QBO), which was the dominant mode of Asian monsoon variation on an interannual scale [54]. The QBO could modulate the variability of the equatorial stratosphere by alternating descending regimes of easterly and westerly zonal winds, with a variable period averaging approximately 28 months [55]. The QBO could also influence the El Niño–Southern Oscillation (ENSO) and precipitation in China by changing the position and intensity of abnormal cyclones (anticyclones) in the Philippines [56]. A possible connection with the QBO is supported by the significantly negative correlation between the reconstructed $SPEI_{82}$ and the QBO from April of the previous year (https://psl.noaa.gov/data/correlation/qbo.data, accessed on 16 January 2022), with $r = -0.205$ ($p < 0.105$, $N = 64$, 1948–2012). An 11-year moving average was used to calculate a correlation coefficient of -0.327 ($p < 0.016$). The significant peaks at 3.36 years and 3.59 years were within the 3–7 year range of the ENSO cycle, which could have had a strong influence on precipitation in and around northern China by modulating the strength of the Asian summer monsoon [57]. During El Niño's mature phase in winter, the meridionality of atmospheric activity is enhanced at middle–high latitudes, the Aleutian low–high-pressure ridge is strengthened over Lake Baikal and northerly winds prevail with less rainfall in northern China [58]. Previous studies have reported that ENSO events influence the climate of China via zonal and meridional heat transport [57,58]. Furthermore, on a decadal scale, the $SPEI_{82}$ reconstruction was significantly correlated with the Southern Oscillation Index (SOI) and the Niño 1 + 2 Index from July of the previous year, and the Niño 3 index and the Niño 3.4 index (https://www.esrl.noaa.gov/psd/enso/data.html, accessed on 16 January 2022) from June of the previous year during the period from 1908–2007, with correlation coefficients of 0.341 ($p < 0.001$), -0.445 ($p < 0.001$), -0.706 ($p < 0.001$) and -0.603 ($p < 0.001$), respectively. The multidecadal cycles of 18.62 years possibly corresponded to the periods of approximately 20–30 Pacific decadal oscillations (PDOs) [59], which could affect the distribution of precipitation in China [60] by changing the location of the subtropical high and the strength of the summer monsoon. In the warm phases of PDO, because of the strong influence of anomalous high pressure and anticyclonic systems in the mid–lower troposphere, severe droughts often occurred in both North and South China, and severe floods often occurred in the middle and lower Yangtze River Valley. The opposite variations occurred in the cold phases of the PDO [61]. A strong negative correlation between the reconstructed $SPEI_{82}$ series and the PDO (https://www.esrl.noaa.gov/psd/enso/data.html, accessed on 16 January 2022) from February of the current year ($r = -0.285$, $N = 100$, $p < 0.004$, 1908–2007), the reconstructed PDO [62] ($r = -0.315$, $N = 79$, $p < 0.005$,1908–1986) and the annual PDO [63] ($r = -0.369$, $N = 84$, $p < 0.001$, 1908–1991) on an interdecadal timescale confirmed the relationship. The results above indicated that the moisture conditions in northern North China may be influenced by the QBO, ENSO and PDO. The influence of the QBO, ENSO and PDO on tree growth in Asia has also been detected in other studies based on tree rings in northern China [16,64–66]. Furthermore, the reconstructed $SPEI_{82}$ and ENSO (such as SOI, Niño 1 + 2, Niño 3 and Niño 3.4 Index) showed similar variation trends on a decadal scale (Figure 10). Significantly negative (positive) correlation of the reconstructed $SPEI_{82}$ with the sea surface temperatures (SSTs) from May to November of the previous year in the eastern equatorial Pacific Ocean (Southeast Pacific Ocean) (Figure 7c) indicates that ENSO may be the main factor influencing the regional climate. However, the underlying physical mechanisms are not well understood. For a better understanding of the physical mechanisms of hydroclimatic variations, other tree-ring parameters, such as carbon and oxygen stable isotopes and density, should be incorporated in future research.

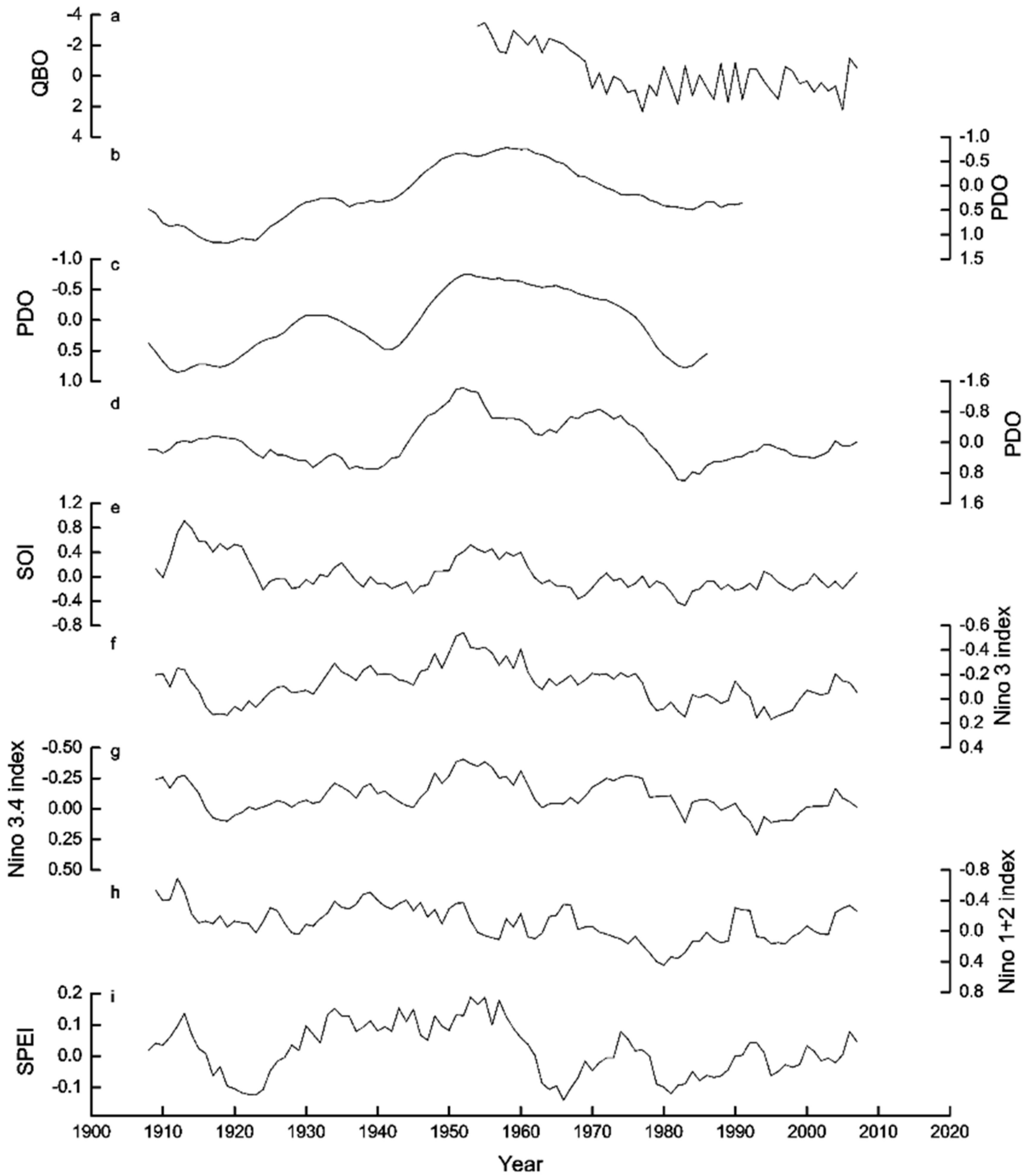

Figure 10. Comparisons with various climate proxies from the Pacific. (**a**) The QBO of from April of the previous year (https://psl.noaa.gov/data/correlation/qbo.data, accessed on 16 January 2022). (**b**) The annual PDO [63]. (**c**) The reconstructed PDO [62]. (**d**) The PDO from February of the current year (https://www.esrl.noaa.gov/psd/enso/data.html, accessed on 16 January 2022). (**e**) The SOI from July of the previous year. (**f**) The Niño 1 + 2 Index from July of the previous year. (**g**) The Niño 3 Index from June of the previous year. (**h**) The Niño 3.4 Index from June of the previous year (https://www.esrl.noaa.gov/psd/enso/data.html, accessed on 16 January 2022). (**i**) The $SPEI_{82}$ reconstruction in this study. All of the lines represent an 11-year moving average.

5. Conclusions

Using tree-ring width RES chronology developed from Chinese pines, the SPEI from August of the previous year to February of the current year from 1903–2012 was reconstructed in northern North China. Five dry periods and three wet periods lasting over three years were observed during the reconstructed period. Most of the dry years (periods) were confirmed by drought events from historical records. The results of the comparison analysis indicated that the reconstructed $SPEI_{82}$ series could reflect a large-scale hydroclimatic signal in the northern part of China. Significant periodicities were found in the $SPEI_{82}$ reconstruction, and significant correlations existed between the reconstructed data and other indices (including the QBO, ENSO and PDO) on a decadal scale, indicating that the $SPEI_{82}$ reconstruction in northern China might be strongly influenced by extensive atmosphere–sea interactions. Drought variations in the study area significantly correlated with SSTs in the eastern equatorial Pacific Ocean (Southeast Pacific Ocean), suggesting a possible connection of regional hydroclimatic variations to the ENSO. However, further research needs to be performed to investigate the mechanisms underlying these interactions.

Author Contributions: Conceptualization, Y.W. and H.Z.; methodology, Y.W. and H.Z.; software, Y.W.; validation, Y.W., H.Z. and H.W. (Hui Wang); investigation, Y.W., H.Z., H.W. (Hui Wang), J.G., E.Z., J.W., X.L., H.W. (Haoliang Wei) and C.Z.; resources, Y.W.; data curation, Y.W., H.Z. and H.W. (Hui Wang); writing—original draft preparation, Y.W.; writing—review and editing, Y.W. and H.Z.; visualization, Y.W. and H.W. (Hui Wang); supervision, H.Z.; project administration, Y.W. and H.Z.; Y.W. and H.Z. have contributed equally to this work. All authors have read and agreed to the published version of the manuscript.

Funding: This research was funded by the higher education scientific and technology research project in Hebei Province (QN2019318, ZD2019303), the Natural Science Foundation of Hebei Province (D2016108005), the State Key Laboratory of Loess and Quaternary Geology Foundation (SKLLQG1720) and the science and technology planning projects from Xingtai Technology Bureau (2021ZZ026). The funders had no role in study design, data collection and analysis, decision to publish or preparation of the manuscript.

Institutional Review Board Statement: Not applicable.

Informed Consent Statement: Not applicable.

Data Availability Statement: The reconstructed August–February SPEI series were uploaded as the Supporting Information. The precipitation and temperature data were collected from the China Meteorological Data Sharing Service System (http://data.cma.cn/en, accessed on 16 January 2022). The mean temperature data for the SPEI drought monitor were from the NOAA NCEP CPC GHCN_CAMS gridded dataset (https://ftp.cpc.ncep.noaa.gov/wd51yf/GHCN_CAMS/, accessed on 16 January 2022) and the monthly precipitation data for the SPEI drought monitor were from the Global Precipitation Climatology Centre (GPCC) (http://climexp.knmi.nl, accessed on 16 January 2022). The long-term instrumental precipitation records from the Beijing meteorological station were collected from http://climexp.knmi.nl, accessed on 16 January 2022. The scPDSI data were collected from https://www.uea.ac.uk/web/groups-and-centres/climatic-research-unit/data, accessed on 18 December 2021. The SPEI data were collected from http://sac.csic.es/spei/index.html, accessed on 16 January 2022.

Conflicts of Interest: The authors declare no conflict of interest.

References

1. Jackson, L.S.; Crook, J.A.; Forster, P.M. An intensified hydrological cycle in the simulation of geoengineering by cirrus cloud thinning using ice crystal fall speed changes. *J. Geophys. Res. Atmos.* **2016**, *121*, 6822–6840. [CrossRef]
2. Trenberth, K.E. Attribution of climate variations and trends to human influences and natural variability. *WIREs Clim. Change* **2011**, *2*, 925–930. [CrossRef]
3. Vizy, E.; Cook, K. Mid-Twenty-First-Century Changes in Extreme Events over Northern and Tropical Africa. *J. Clim.* **2012**, *25*, 5748–5767. [CrossRef]
4. Zhang, R.; Shang, H.; Yu, S.; He, Q.; Yuan, Y.; Bolatov, K.; Mambetov, B.T. Tree-ring-based precipitation reconstruction in southern Kazakhstan, reveals drought variability since A.D. 1770. *Int. J. Climatol.* **2017**, *37*, 741–750. [CrossRef]
5. Zhang, R.; Qin, L.; Yuan, Y.; Gou, X.; Zou, C.; Yang, Q.; Shang, H.; Fan, Z. Radial growth response of *Populus xjrtyschensis* to environmental factors and a century-long reconstruction of summer streamflow for the Tuoshigan River, northwestern China. *Ecol. Indic.* **2016**, *71*, 191–197. [CrossRef]
6. Yuan, Z.; Yan, D.; Yang, Z.; Yin, J.; Yuan, Y. Temporal and spatial variability of drought in Huang-Huai-Hai River Basin, China. *Theor. Appl. Climatol.* **2014**, *122*, 755–769. [CrossRef]
7. Mcdowell, N.G.; Allen, C.D. Darcy's law predicts widespread forest mortality under climate warming. *Nat. Clim. Change* **2015**, *5*, 669–672. [CrossRef]

8. Liu, Y.; Wang, C.Y.; Hao, W.J.; Song, H.M.; Cai, Q.F.; Tian, H.; Sun, B.; Linderholm, H.W. Tree-ring-based annual precipita-tion reconstruction in Kalaqin, Inner Mongolia for the last 238 years. *Chin. Sci. Bull.* **2011**, *56*, 2995–3002. [CrossRef]
9. Wang, Y.; Liu, Y.; Zhang, H.; Wang, H.; Guo, J.; Zhang, E.; Wang, J.; Li, X. Temperature variability inferred from tree-ring records in Weichang region, China, and its teleconnection with large-scale climate forcing. *Clim. Dyn.* **2019**, *52*, 1533–1545. [CrossRef]
10. Ma, Y.; Liu, Y.; Song, H.; Sun, J.; Lei, Y.; Wang, Y. A Standardized Precipitation Evapotranspiration Index Reconstruction in the Taihe Mountains Using Tree-Ring Widths for the Last 283 Years. *PLoS ONE* **2015**, *10*, e0133605. [CrossRef]
11. Vicente-Serrano, S.; Beguería, S.; López-Moreno, J.I. A Multiscalar Drought Index Sensitive to Global Warming: The Standardized Precipitation Evapotranspiration Index. *J. Clim.* **2010**, *23*, 1696–1718. [CrossRef]
12. Nakanyete, N.; Shikangalah, R.N.; Vatuva, A. Drought as a Disaster in the Namibian Context. *Int. J. Sci. Res.* **2020**, *9*, 377–386.
13. Dai, A.; Trenberth, K.E.; Qian, T.T. A global dataset of Palmer Drought Severity Index for 1870-2002, Relationship with soil moisture and effects of surface warming. *J. Hydrometeorol.* **2004**, *5*, 1117–1130. [CrossRef]
14. Ionita, M.; Scholz, P.; Chelcea, S.M. Spatio-temporal variability of dryness/wetness in the Danube River Basin, Drought Variability Danube. *Hydrol. Process.* **2015**, *29*, 4483–4497. [CrossRef]
15. Du, J.; Fang, J.; Xu, W.; Shi, P. Analysis of dry/wet conditions using the standardized precipitation index and its potential usefulness for drought/flood monitoring in Hunan Province, China. *Stoch. Environ. Res. Risk A* **2013**, *27*, 377–387. [CrossRef]
16. Wang, Y.; Liu, Y. Reconstruction of March–June precipitation from tree rings in central Liaoning, China. *Clim. Dyn.* **2017**, *49*, 3111–3121. [CrossRef]
17. Peng, J.; Sun, Y.; Chen, M.; He, X.; Davi, N.; Zhang, X.; Li, T.; Zhu, C.; Cai, C.; Chen, Z.J. Tree-ring based precipitation variability since AD 1828 in northwestern Liaoning, China. *Quat. Int.* **2013**, *283*, 63–71. [CrossRef]
18. Liu, Y.; Tian, H.; Song, H.M.; Liang, J.M. Tree ring precipitation reconstruction in the Chifeng-Weichang region, China, and East Asian summer monsoon variation since AD 1777. *J. Geophys. Res. Atmos.* **2010**, *115*, D06103.
19. Liu, Y.; Song, H.; Sun, C.; Song, Y.; Cai, Q.; Liu, R.; Lei, Y.; Li, Q. The 600-mm precipitation isoline distinguishes tree-ring width responses to climate in China. *Natl. Sci. Rev.* **2018**, *6*, 359–368. [CrossRef]
20. Li, Q.; Liu, Y.; Nakatsuka, T.; Song, H.; McCarroll, D.; Yang, Y.; Qi, J. The 225-year precipitation variability inferred from tree-ring records in Shanxi Province, the North China, and its teleconnection with Indian summer monsoon. *Glob. Planet Change* **2015**, *132*, 11–19. [CrossRef]
21. Fan, Z.; Thomas, A. Decadal changes of reference crop evapotranspiration attribution, spatial and temporal variability over China 1960–2011. *J. Hydrol.* **2018**, *560*, 461–470. [CrossRef]
22. Abiodun, B.J.; Salami, A.T.; Matthew, O.J.; Odedokun, S. Potential impacts of afforestation on climate change and extreme events in Nigeria. *Clim. Dyn.* **2013**, *41*, 277–293. [CrossRef]
23. Li, L.; She, D.; Zheng, H.; Lin, P.; Yang, Z. Elucidating Diverse Drought Characteristics from Two Meteorological Drought Indices (SPI and SPEI) in China. *J. Hydrometeorol.* **2020**, *21*, 1513–1530. [CrossRef]
24. Sisay, A.; Ayoade, J.; Bello, N. Comparative analyses of SPI and SPEI as drought assessment tools in Tigray Region, Northern Ethiopia. *SN Appl. Sci.* **2019**, *1*, 1265.
25. Liu, N.; Liu, Y.; Bao, G.; Bao, M.; Wang, Y.; Zhang, L.; Ge, Y.; Bao, W.; Tian, H. Drought reconstruction in eastern Hulun Buir steppe, China and its linkages to the sea surface temperatures in the Pacific Ocean. *J. Asian Earth Sci.* **2016**, *115*, 298–307. [CrossRef]
26. Chen, F.; Yuan, Y.; Yu, S.; Zhang, T.; Shang, H.; Zhang, R.; Qin, L.; Fan, Z. A 225-year long drought reconstruction for east Xinjiang based on Siberia larch (*Larix sibirica*) tree-ring widths, Reveals the recent dry trend of the eastern end of Tien Shan. *Quat. Int.* **2015**, *358*, 42–47. [CrossRef]
27. Martin-Benito, D.; Beeckman, H.; Cañellas, I. Influence of drought on tree rings and tracheid features of *Pinus nigra* and *Pinus sylvestris* in a mesic Mediterranean forest. *Eur. J. For. Res.* **2013**, *132*, 33–45. [CrossRef]
28. Ram, S.; Singh, H.; Yadav, R.; Varikoden, H.; Nandargi, S.; Srivastava, M. Variations in vapor pressure and standardized precipitation evapotranspiration index since AD 1861 over the western Himalaya in India, inference from tree ring-width records. *Theor. Appl. Climatol.* **2020**, *140*, 157–166. [CrossRef]
29. Allen, K.; Freund, M.; Palmer, J.; Simkin, R.; Williams, L.; Brookhouse, M.; Cook, E.; Stewart, S.; Baker, P. Hydroclimate extremes in a north Australian drought reconstruction asymmetrically linked with Central Pacific Sea surface temperatures. *Glob. Planet Change* **2020**, *195*, 103329. [CrossRef]
30. Chu, X.; Zhan, J.; Wang, C.; Hameeda, S.; Wang, X. Households' Willingness to Accept Improved Ecosystem Services and Influencing Factors: Application of Contingent Valuation Method in Bashang Plateau, Hebei Province, China. *J. Environ. Manag.* **2020**, *255*, 109925. [CrossRef]
31. Cook, E.R.; Kairiukstis, L.A. *Methods of Dendrochronology*; Kluwer Academic Publishers: Dordrecht, The Netherlands, 1990; pp. 1–391.
32. Fritts, H.C. *Tree Rings and Climate*; Blackburn Press: Caldwell, NJ, USA, 2001; pp. 1–567.
33. Holmes, R.L. Computer-assisted quality control in tree-ring dating and measurement. *Tree-Ring Bull.* **1983**, *43*, 69–78.
34. Cook, E.R.; Holmes, R.L. *Users Manual for Program ARSTAN*; Laboratory of Tree-Ring Research, University of Arizona: Tucson, AZ, USA, 1986; pp. 50–56.
35. Gazol, A.; Camarero, J.; Gutiérrez, E.; Ionel, P.; Andreu-Hayles, L.; Motta, R.; Nola, P.; Ribas, M.; Sangüesa-Barreda, G.; Urbinati, C.; et al. Distinct effects of climate warming on populations of silver fir (*Abies alba*) across Europe. *J. Biogeogr.* **2015**, *42*, 1150–1162. [CrossRef]

36. Wigley, T.M.L.; Briffa, K.R.; Jones, P.D. On the average value of correlated time series, with application in dendroclimatology and hydrometeorology. *J. Appl. Meteorol. Clim.* **1984**, *23*, 201–213. [CrossRef]
37. Schrier, G.; Barichivich, J.; Briffa, K.; Jones, P. A scPDSI-based global data set of dry and wet spells for 1901–2009. *J. Geophys. Res. Atmos.* **2013**, *118*, 4025–4048. [CrossRef]
38. Proutsos, N.; Tigkas, D. Growth Response of Endemic Black Pine Trees to Meteorological Variations and Drought Episodes in a Mediterranean Region. *Atmosphere* **2020**, *11*, 554. [CrossRef]
39. Vieira, J.; Nabais, C.; Campelo, F. Extreme Growth Increments Reveal Local and Regional Climatic Signals in Two Pinus pinaster Populations. *Front. Plant Sci.* **2021**, *12*, 658777. [CrossRef]
40. Cook, E.R.; Meko, D.M.; Stahle, D.W.; Cleaveland, M.K. Drought reconstructions for the continental United States. *J. Clim.* **1999**, *12*, 1145–1162. [CrossRef]
41. Fritts, H.C. *Reconstructing Large-Scale Climatic Patterns from Tree-Ring Data*; The University of Arizona Press: Tucson, AZ, USA, 1991; p. 286.
42. Liu, N.; Liu, Y.; Bao, G.; Bao, M.; Wang, Y.; Ge, Y.; Zhang, L.; Bao, W.; Tian, H. A tree-ring based reconstruction of summer relative humidity variability in eastern Mongolian Plateau and its associations with the Pacific and Indian Oceans. *Palaeogeogr. Palaeoclimatol. Palaeoecol.* **2015**, *438*, 113–123. [CrossRef]
43. Cai, Q.; Liu, Y.; Wang, Y.; Ma, Y.; Liu, H. Recent warming evidence inferred from a tree-ring-based winter-half year minimum temperature reconstruction in northwestern Yichang, South Central China, and its relation to the large-scale circulation anomalies. *Int. J. Biometeorol.* **2016**, *60*, 1885–1896. [CrossRef]
44. Cook, E.R.; Esper, J.; D'Arrigo, R.D. Extra-tropical Northern Hemisphere land temperature variability over the past 1000 years. *Quat. Sci. Rev.* **2004**, *23*, 2063–2074. [CrossRef]
45. Loader, N.; Young, G.; McCarroll, D.; Wilson, R. Quantifying uncertainty in isotope dendroclimatology. *Holocene* **2013**, *23*, 1221–1226. [CrossRef]
46. Rossi, S.; Morin, H.; Deslauriers, A. Multi-scale Influence of Snowmelt on Xylogenesis of Black Spruce. *Arct. Antarct. Alp. Res.* **2011**, *43*, 457–464. [CrossRef]
47. Mäkinen, H.; Nöjd, P.; Mielikäinen, K. Climatic signal in annual growth variation in damaged and healthy stands of Norway spruce [*Picea abies* (L.) Karst.] in southern Finland. *Trees* **2001**, *15*, 177–185. [CrossRef]
48. Academy of Meteorological Science. *Yearly Charts of Dryness/Wetness in China for the Last 500-Year Period*; Maps Press: Beijing, China, 1981; pp. 1–332. (In Chinese)
49. Zhang, D.; Li, X.; Liang, Y. The sequel "Yearly charts of Dryness/Wetness in China for the last 500-year period (1993–2000AD)". *J. Appl. Meteorol. Sci.* **2003**, *14*, 379–388. (In Chinese) [CrossRef]
50. Zhang, D.; Liu, C. The sequel "Yearly charts of Dryness/Wetness in China for the last 500-year period (1980–1992AD)". *Meteorol. Mon.* **1993**, *19*, 41–45. (In Chinese)
51. Xu, Y.; Shao, X.; Liu, J. Research on historical characteristics of flooding and drought in Hebei province. *J. Catastrophol.* **2001**, *16*, 53–57. (In Chinese)
52. Zhang, Q. The variations of the precipitation and water resources in north china since 1880. *Plateau Meteorol.* **1999**, *18*, 486–495. (In Chinese)
53. Liang, E.; Liu, X.; Yuan, Y.; Qin, N.; Fang, X.; Huang, L.; Zhu, H.; Wang, L.; Shao, X. The 1920S Drought Recorded by Tree Rings and Historical Documents in the Semi-Arid and Arid Areas of Northern China. *Clim. Change* **2006**, *79*, 403–432. [CrossRef]
54. Ding, Y. The variability of the Asian summer monsoon. *J. Meteorol. Soc. Jpn.* **2007**, *85*, 21–54. [CrossRef]
55. Butler, A.; Charlton-Perez, A.; Domeisen, D.I.V.; Garfinkel, C.; Gerber, E.P.; Hitchcock, P.; Karpechko, A.Y.; Maycock, A.C.; Sigmond, M.; Simpson, I.; et al. Chapter 11—Sub-seasonal Predictability and the Stratosphere. In *Sub-Seasonal to Seasonal Prediction*; Robertson, A.W., Vitart, F., Eds.; Elsevier: Amsterdam, The Netherlands, 2019; pp. 223–241.
56. Liu, C.; Rao, J.; Wu, Z.; Hu, J.; Ma, X. Linkage between ENSO and China Summer Rainfall, Modulation by QBO. *J. Trop. Meteorol.* **2019**, *35*, 210–223. (In Chinese)
57. Xu, H.; Hong, Y.; Hong, B.; Zhu, Y.; Wang, Y. Influence of ENSO on multi-annual temperature variations at Hongyuan, NE Qinghai-Tibet plateau, evidence from $\delta^{13}C$ of spruce tree rings. *Int. J. Climatol.* **2010**, *30*, 120–126. [CrossRef]
58. Chen, Y.; Zhao, Y.; Feng, J.; Wang, F. ENSO cycle and climate anomaly in China. *Chin. J. Oceanol. Limnol.* **2012**, *30*, 985–1000. [CrossRef]
59. Gedalof, Z.E.; Mantua, N.J.; Peterson, D.L. A multi-century perspective of variability in the Pacific Decadal Oscillation, new insights from tree rings and coral. *Geophys. Res. Lett.* **2002**, *29*, 2204. [CrossRef]
60. Lin, F.; Tan, L.; Xue, G.; Cheng, X.; Zhang, H.; Cheng, H.; Edwards, R.L.; Wang, T.; Li, D.; Gao, Y.; et al. Seasonality of precipitation recorded in a modern (1907–2008) annually laminated stalagmite from central China. *Palaeogeogr. Palaeoclimatol. Palaeoecol.* **2021**, *576*, 110489. [CrossRef]
61. Shen, C.M.; Wang, W.C.; Gong, W.; Hao, Z.X. A Pacific Decadal Oscillation record since 1470 AD reconstructed from proxy data of summer rainfall over eastern China. *Geophys. Res. Lett.* **2006**, *33*, L03702. [CrossRef]
62. Biondi, F.; Gershunov, A.; Cayan, D.R. North Pacific decadal climate variability since 1661. *J. Clim.* **2001**, *14*, 5–10. [CrossRef]
63. MacDonald, G.M.; Case, R.A. Variations in the Pacific Decadal Oscillation over the past millennium. *Geophys. Res. Lett.* **2005**, *32*, L08703. [CrossRef]

64. Bao, G.; Liu, Y.; Liu, N.; Linderholm, H.W. Drought variability in eastern Mongolian Plateau and its linkages to the large-scale climate forcing. *Clim. Dyn.* **2015**, *44*, 717–733. [CrossRef]
65. Liu, Y.; Zhang, X.; Song, H.; Cai, Q.; Li, Q.; Zhao, B.; Liu, H.; Mei, R. Tree-ring-width-based PDSI reconstruction for central Inner Mongolia, China over the past 333 years. *Clim. Dyn.* **2016**, *48*, 867–879. [CrossRef]
66. Liu, R.; Liu, Y.; Li, Q.; Song, H.; Li, X.; Sun, C.; Cai, Q.; Song, Y. Seasonal Palmer drought severity index reconstruction using tree-ring widths from multiple sites over the central-western Da Hinggan Mountains, China since 1825 AD. *Clim. Dyn.* **2019**, *53*, 3661–3674. [CrossRef]